Lee, F. H., Juneja, A. & Tan, T. S. (2004). *Géotechnique* **54**, No. 1, 1–16

Stress and pore pressure changes due to sand compaction pile installation in soft clay

F. H. LEE*, A. JUNEJA† and T. S. TAN*

This paper presents centrifuge model data and describes a semi-empirical approach to predict short-term total radial stress and pore pressure changes around sand compaction piles installed in soft marine clays. Comparison of the measured changes in radial stress and pore pressure with plane strain cavity expansion theory shows that the latter gives a reasonably good estimate at large depth for the entire installation process and for the peak stress measured during casing jack-in, but not for the residual stress after casing jack-in. However, deviation from plane strain cavity expansion theory was noted at shallow depths. To account for the effect of the ground surface, a plane stress cavity expansion theory was proposed for the shallow zones, which assumes constant vertical overburden stress. The establishment of the two limits formed by the plane strain and plane stress theories allows semi-empirical relations to be established by fitting to the data. These semi-empirical relations allow the post-installation and peak jack-in stress and pore pressure to be reasonably estimated. However, post-jack-in values remain significantly overestimated. These findings imply that, in order to mobilise significant set-up of stress in the improved ground, there must be substantial further cavity expansion during the sand injection stage of SCP. Cumulative total stress increment at a given location due to the installation of multiple piles in a grid may be reasonably estimated by superimposing the increments due to the installation of each pile. On the other hand, pore pressure build-up is shown to be less readily superimposed, possibly because the shear-induced component of excess pore pressure does not increase linearly and infinitely with deviator stress.

KEYWORDS: bearing capacity; centrifuge modelling; ground improvement; shear strength; clay; model tests

Cet exposé présente des données de modèle centrifuge et décrit une approche semi-empirique pour prévoir à court terme la contrainte totale radiale et les changements de pression interstitielle autour des piles de compaction de sable installées dans des argiles marines tendres. La comparaison des changements mesurés de contrainte radiale et de pression interstitielle avec la théorie d'expansion de cavité à déformation plane montre que cette dernière donne une estimation relativement bonne à grande profondeur pour tout le processus d'installation et pour la contrainte de crête mesurée pendant l'enfoncement du casing mais pas pour la contrainte résiduelle après l'enfoncement du casing. Cependant, un écart avec la théorie d'expansion de cavité à déformation plane a été noté à faible profondeur. Pour expliquer les effets de la surface du sol, une théorie d'expansion de cavité à déformation plane a été proposée pour les zones de faible profondeur, ce qui suppose une contrainte de surcharge verticale constante. L'établissement de deux limites formées par les théories de déformation plane et de contrainte plane permet d'établir des relations semi-empiriques en suivant les données. Ces relations semi-empiriques permettent de faire une évaluation raisonnable de la contrainte et de la pression interstitielle de post-installation et de crête. Cependant, les valeurs post-enfoncement restent trop surestimées. Ces résultats impliquent que, afin de mobiliser une contrainte significative dans le sol amélioré, il faut qu'il y ait une expansion de cavité supplémentaire substantielle pendant le stade d'injection de sable du SCP. Une augmentation cumulative totale de la contrainte à un endroit donné, en raison de l'installation de piles multiples dans une grille, peut être raisonnablement évaluée en surimposant les augmentations dues à l'installation de chaque pile. D'un autre côté, nous montrons que les accumulations de pression interstitielle sont moins facilement surimposées, peut-être parce que le composant dû au cisaillement de la pression de pore excessive n'augmente pas de manière linéaire et à l'infini avec une contrainte déviatrice.

INTRODUCTION

Sand compaction piles (SCPs) are commonly used for rapid stabilisation of soft seabeds in near-shore construction works (e.g. Aboshi & Suematsu, 1985). In the field, an SCP is usually installed by driving a steel casing containing sand to the required depth. By repeatedly withdrawing the casing and then re-driving it downwards for part of the withdrawal stroke, the sand is alternately discharged and compressed, thereby resulting in a well-compacted sand pile with a diameter larger than that of the casing (Aboshi *et al.*, 1979).

Manuscript received 17 September 2002, revised manuscript accepted 24 October 2003.
Discussion on this paper closes 1 July 2004, for further details see p. ii.
* Department of Civil Engineering, National University of Singapore.
† Geotest Consultants India, New Delhi, India.

The process of SCP installation has been known to affect the strength of the in-situ clay. Enokido *et al.* (1973) observed that the post-installation unconfined compressive strength of the clay was about two times the pre-installation strength. Aboshi *et al.* (1979) also observed the strength of soft clay to increase by about 50% after the installation as the excess pore pressure dissipated. Asaoka *et al.* (1994) also noted a similar set-up in strength at every depth in a field test. Using finite element analysis, they showed that this increase in strength can be explained by an increase in the effective stress of the clay, caused by the set-up in stresses induced by the SCP installation process.

In spite of this, current design guidelines (e.g. Aboshi *et al.*, 1979, 1991) do not consider the increase in strength of the soft clay that takes place upon SCP installation. This is due to the fact that little is known about the magnitude of these stress and pore pressure changes in the soft clay during

SCP installation. The large ground displacement caused by SCP installation makes stress measurement within the soft clay difficult and unreliable. This displacement effect is also seldom simulated in centrifuge model tests. In most of the centrifuge model studies to date, SCPs were installed using either the frozen pile method, in which frozen columns of sand are pushed into pre-drilled holes at 1 *g* (e.g. Kimura *et al.*, 1985; Kitazume *et al.*, 1996), or by pouring dry sand into the holes in the model soil beds (e.g. Almeida *et al.*, 1985; Takada *et al.*, 1988). Neither of these methods is able to simulate the displacement effect in the surrounding soft clay. Lee *et al.* (2001) examined the performance of SCPs installed using three different methods: the frozen pile method, a 1 *g* displacement method that involves forcibly injecting sand into a soft clay bed at 1 *g* (Lee *et al.*, 1996), and a high-*g* displacement method that involves forcibly injecting sand into a soft clay bed at high-*g* (Ng *et al.*, 1998). They noted that the composite strength and stiffness of a soft ground improved by model SCPs formed by the displacement methods are significantly higher than those formed by the frozen pile method. Using centrifuge model tests, Lee *et al.* (2002a) presented some data on excess pore pressure after the SCP installation and suggested that the excess pore pressure can be approximately described by the plane strain cavity expansion theory (CET) (e.g. Gibson & Anderson, 1961; Vesic, 1972), together with an empirical constant to account for the deviation from the plane strain condition near the ground surface. However, in assessing the effects of set-up in strength of the soft clay, measurement of changes in total stress is also required in addition to the measurement of pore pressure changes.

This paper examines the short-term changes in radial stress and pore pressure due to the installation of SCPs in soft clay, using data obtained from centrifuge model tests. The centrifuge model tests conducted in this study are described first. The horizontal stress and pore pressure measurements observed during jack-in of the casing and the entire installation process of a single SCP are then compared with several variations of the CET, leading to the proposal of a semi-empirical method that allows stress and pore pressure changes to be determined. The stress and pore pressure changes arising from the installation of pile groups are then examined, leading to a simple superposition method for estimating the short-term changes in horizontal stress and pore pressure in SCP groups. All dimensions in the figures are in mm unless stated.

EXPERIMENTAL ASPECTS

The model tests were conducted on the National University of Singapore (NUS) Geotechnical Centrifuge using the in-flight SCP installer (Ng *et al.*, 1998). The soft clay used in all these tests is remoulded and reconsolidated Singapore marine clay, the properties of which are summarised in Table 1. The soft clay beds were housed within strongboxes, each having internal dimensions of 520 mm × 255 mm × 250 mm. The inside walls of the strongbox were first coated with high-vacuum silicone grease, and perforated flexible tubing laid over its base to facilitate drainage during consolidation. The tubing was then covered with a 5 mm-thick sand layer. A sheet of propylene non-woven geotextile was also placed to provide a filter barrier in between the sand layer and the clay slurry. De-aired clay slurry with water content of about 1·5 times the liquid limit was then placed into the container. The slurry was then allowed to consolidate on the laboratory floor, first under its own self-weight and later under a surcharge of 6 kPa on the clay surface.

Table 1. Properties of Singapore marine clay

Property	Value
Water content: %	70·0
Bulk unit weight: kN/m^3	15·6
Liquid limit: %	86·5
Plastic limit: %	31·5
Specific gravity	2·65
Free swell index: %	31·3

After the completion of surcharge consolidation, the model clay beds were consolidated using vacuum-induced downward seepage (Robinson *et al.*, 2003). A vacuum suction of 335 mmHg was applied to the bottom of the sample to induce downward seepage. The level of the vacuum was set so as to achieve an effective stress gradient in the clay similar to that obtained at the 70 *g* model gravity. As Robinson *et al.* (2003) showed, this method of vacuum-induced consolidation produces an undrained shear strength profile that agrees reasonably well with that obtained by high-*g* self-weight consolidation.

Upon completion of the vacuum suction consolidation at 1 *g*, the sides of the strongbox were removed and holes drilled into the sides of the clay bed at prescribed locations using drill-bits. The removal of the vacuum suction is likely to result in some swelling of the clay bed. Observations show that the heave due to swelling is negligible, being less than 1 mm in most cases. This is in agreement with the estimated heave based on consolidation theory and the swelling modulus of the marine clay. Thus the effect of swelling on the locations of the sensors is negligible. The stress state of the clay bed after swelling also does not pose any problems, as the clay bed will subsequently be re-consolidated at 70*g* model gravity before the model SCPs are installed. Total stress transducers (TSTs) and pore pressure transducers (PPTs) were inserted into these holes and the latter were subsequently grouted up with marine clay slurry at 1·5 times the liquid limit. During insertion, the orientation of the TST diaphragm was held vertical so as to measure the horizontal stress. Entran EPL-D12 TSTs and Druck PDCR81 PPTs were used in the tests. The performance of these transducers has been reported by Konig *et al.* (1994) and Lee *et al.* (2002b), and will not be repeated herein.

The EPL-D12 TSTs were waterproofed by coating them with a thin layer of silicone rubber before insertion into the saturated clay beds. Calibration of the TSTs was conducted in soft clay inside a calibration chamber, under deadweight loading at 1 *g*. As shown in Fig. 1(a), the registration ratio (Weiler & Kulhawy, 1982) of the TST is about 0·7, indicating significant under-reading of the applied stress. Fig. 1(b) shows the corresponding results for the same TST attached to an aluminium plate measuring 7 mm wide × 80 mm long × 1·2 mm thick. As can be seen, the presence of the aluminium backing plate increases the registration ratio of the TST significantly while decreasing the amount of hysteresis between the loading and unloading phases. The reason for this improvement is unclear. One possible reason is that it alters the cell aspect ratio, thereby reducing the stress arching effect over the TST. The plate also helps to reduce the likelihood of the TST rotating during the experiment. Finally, there is also a practical advantage in that more than one TST can be attached to the same plate, which will help to maintain their relative positions. One possible drawback is that the plate may interfere with the soil flow during SCP installation, but this effect was minimised by keeping the width of the plate to a minimum. As shown in Fig. 2, the TST attached to the plate was held vertical before the transducer insertion. After placement of the transducers, the soft clay bed was self-weight consolidated, this time under 70 *g* model gravity, until an average degree of consolidation of at least 95% was achieved.

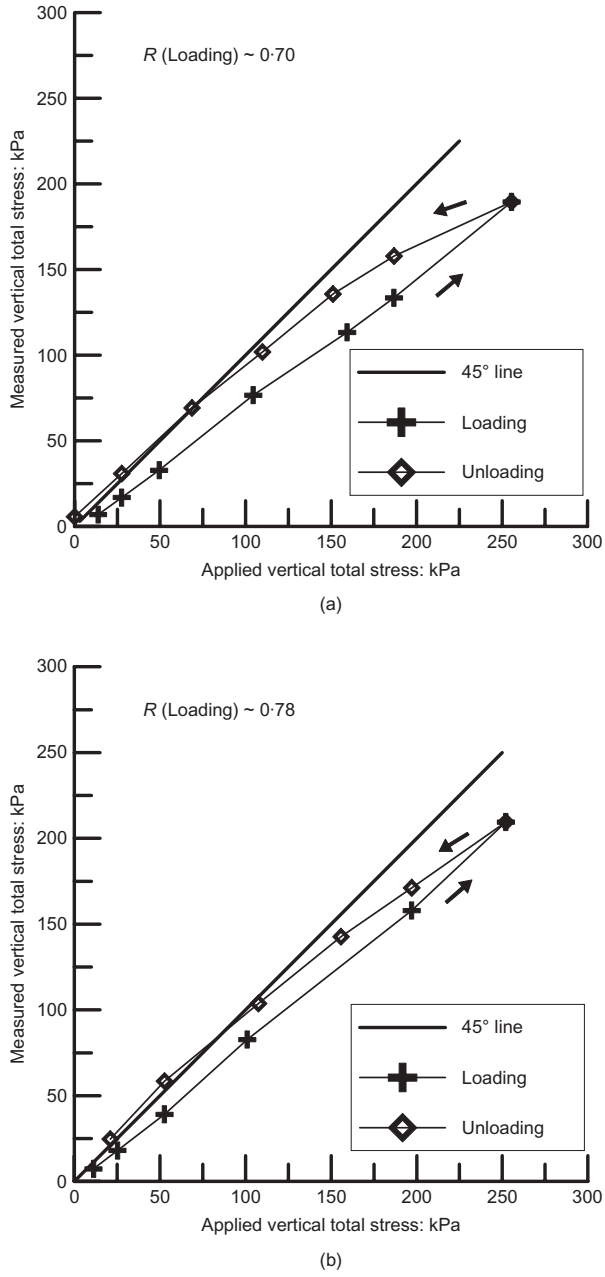

Fig. 1. Vertical loading and unloading cycles on TST in 1*g* calibration tests: (a) without backing plate; (b) with backing plate

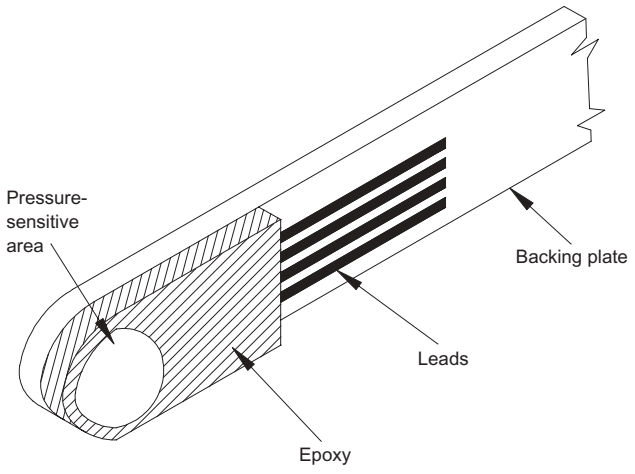

Fig. 2. Entran EPL-D12 total stress transducer with backing plate

The in-flight SCP installer has already been described by Ng *et al.* (1998) and Lee *et al.* (2001), and will not be repeated herein. In essence, this in-flight installation process involves jacking a sand-filled hollow casing of 10 mm internal diameter into a soft clay bed. The jack-in rate varied from 1·2 to 2·4 mm/s in model scale. At the end of the jack-in sequence, the casing was withdrawn at 0·5–1 mm/s while forcibly injecting the sand into the clay bed using an Archimedes screw. The time taken to withdraw the casing could be adjusted to achieve a variable withdrawal rate, thereby allowing SCPs of uniform diameter throughout the depth to be installed. SCPs of 1·6–2 times the diameter of the casing were installed in this method. The relative density of the SCPs so formed is high and of the order of 90%. As no pre-drilled hole exists prior to the installation of the sand pile, the radial displacement undergone by the clay at the edge of the sand pile is equal to the radius of the sand pile. Fig. 3 shows the layout of the SCPs and the transducers in each test. Many of the TSTs were not oriented to measure the radial stress directly. This is because, in each of the tests, more than one SCP is installed. Some of the TSTs were orientated facing the ends or sides of the container rather than any particular piles. Other TSTs were orientated facing one of the SCPs. In cases where more than two SCPs were installed, it is evidently impossible to orientate the TSTs to face all the SCPs. In all these cases, the radial stress was inferred from transducer readings of such TSTs by Mohr circle calculations.

STRESS CHANGES DURING SCP INSTALLATION

The in-flight sand pile installation process comprises casing jack-in followed by sand injection, as the casing is retracted. Typical total horizontal stress and pore pressure measurements during the installation of the first pile in test T6 are shown in Fig. 4. As the figure shows, the casing jack-in caused a gradual build-up in total stress and pore pressure, reaching a peak just as the casing reached the level of the transducers during the jack-in. The magnitude of the peak total horizontal stress and pore pressure decreases with increasing distance from the SCP, and points located beyond 3·6 times the SCP diameter recorded little or no increase in the measured variable. The peaking of the total stress has also been observed in pile jack-in model tests in sand (Leung *et al.*, 2001), and is consistent with the Levadoux & Baligh strain path solution that shows a stress bulb around the tip of the penetrator. Very little pore pressure dissipation occurs during the latent periods between jack-in and sand feed and between successive SCP installation: this is consistent with the low coefficient of consolidation, of about 1 m^2/year, of the Singapore marine clay (Dames & Moore, 1983).

SET-UP DUE TO INSTALLATION OF FIRST SAND PILE

Comparison with plane strain cavity expansion theory

The measured total horizontal stress and pore pressure increase due to the entire process of installation of the first SCP are first compared with values derived from plane strain CET at ultimate state cavity expansion (e.g. Gibson & Anderson, 1961; Vesic, 1972; Yu, 2000). Note that the plane strain CETs of Gibson & Anderson (1961) and Vesic (1972) assume that the initial stress state is isotropic and therefore does not apply strictly to the anisotropic stress state that exists in one-dimensionally normally consolidated clay. Comparison was not made with the Levadoux & Baligh strain path solutions since these solutions clearly do not apply to the sand injection process. In cavity expansion calculations, the soil was assumed to be a linearly elastic, perfectly plastic incompressible material with Young's mod-

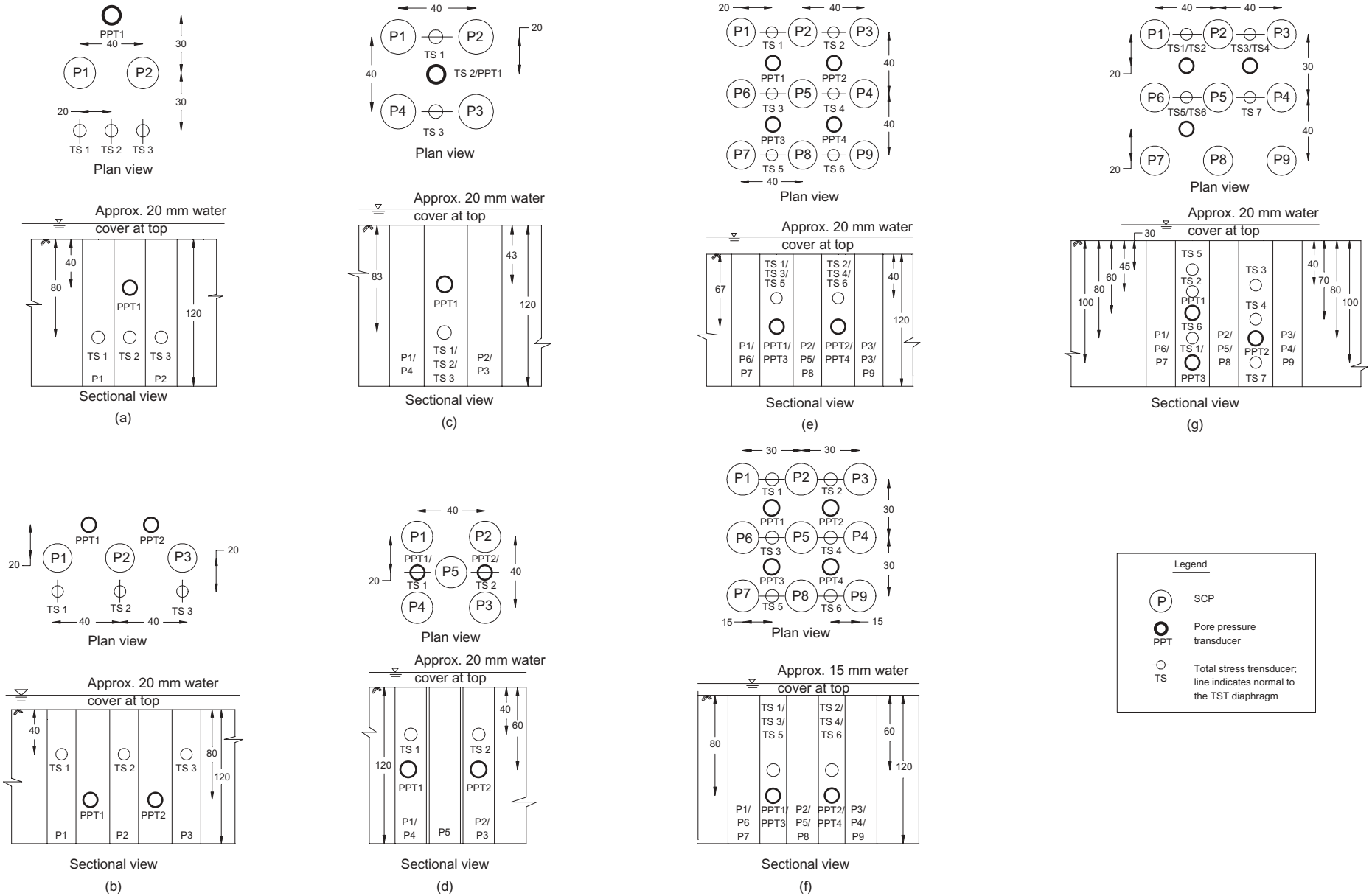

Fig. 3. Layout of SCPs and transducers for tests: (a) T1, $D = 18$ mm; (b) T2, $D = 20$ mm; (c) T3, $D = 16$ mm; (d) T4, $D = 17$ mm; (e) T5, $D = 20$ mm; (f) T6, $D = 20$ mm; (g) T7, $D = 20$ mm (D = SCP diameter)

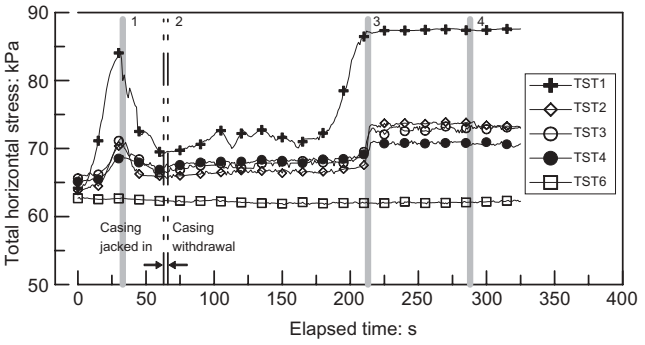

(a)

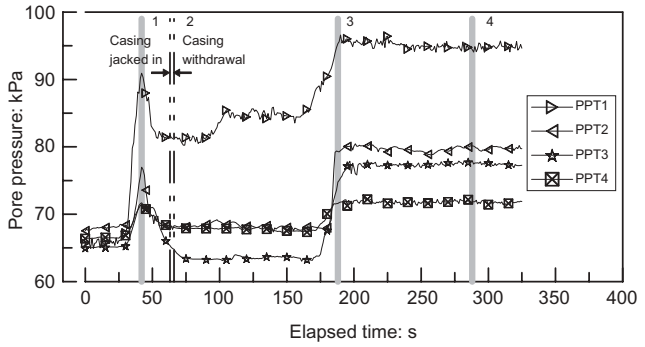

(b)

Fig. 4. Total horizontal stress and pore pressure time history during installation of the SCP in test T6: (a) total stress, TPTs at 60 mm depth; (b) pore pressure, PPTs at 80 mm depth. Line 1: time at which casing tip reaches transducer location during insertion. Line 2: time at which casing tip reaches full penetration and withdrawal starts. Line 3: time at which casing tip reaches transducer location during withdrawal. Line 4: time at end of SCP installation

ulus E_u, yield stress s_u and zero angle of friction. More advanced CETs, such as those based on the Cam clay models (e.g. Yu, 2000; Cao *et al.*, 2001) are available. However, the behaviour of K_0-consolidated soils often does not exactly follow the behaviour that is prescribed by the Cam clay models (e.g. Sekiguchi & Ohta, 1977). Furthermore, Cao *et al.*'s (2001) results indicate that the behaviour of the failure zone—that is, the zone that has reached critical state—is essentially the same as that of the yielded zone in the elastic perfectly plastic model, which is to be expected. The main difference between the predictions of the two material models is that the Cam clay model allows the response of the yielded zone that has not reached critical state to be captured. However, as Cao *et al.*'s (2001) results show, at ultimate state the extent of this zone is relatively small compared with the elastic zone and the failure zone. Thus the modified Cam clay model is unlikely to deviate drastically from the elastic perfectly plastic model.

Figure 5 shows the calculated total horizontal stress normal to the TST diaphragm, and the pore pressure increase, denoted by $\Delta\bar{\sigma}$ and $\Delta\bar{u}$ respectively, after the installation of SCP, plotted against the corresponding measured values, $\Delta\sigma$ and Δu. The orientation of the TST dictated the magnitude of the calculated stress. The calculated total stress was taken equal to the radial total stress if the TST diaphragm radially faced the SCP. Otherwise, the total horizontal stress normal to the diaphragm was computed using the Mohr circle calculations. Dames & Moore (1983) recommended an E_u/s_u value of 200 for Singapore marine clay. Yong *et al.* (1987) also suggested that E_u/s_u for Singapore marine clay lies between 150 and 250. As Figs 5(a) and (b) show, for E_u/s_u of 200 and 150 the calculated total radial stress and pore pressure increase are generally higher than the values inferred from the measurements. As Fig. 5(c) shows, the use of a lower E_u/s_u of 120 clearly improves the matching, but this value of E_u/s_u is substantially lower than that generally recommended for Singapore marine clay.

Figure 6 shows the calculated stress increase normal to the TST diaphragm predicted via plane strain CET and excess pore pressure at the instant of the completion of jack-in with those measured by the transducers. As can be seen, the measured stress ($\Delta\sigma_j$) and excess pore pressure (Δu_j) are generally much smaller than those predicted by plane strain CET. The corresponding calculated values in the figure are represented by $\Delta\bar{\sigma}_j$ and $\Delta\bar{u}_j$ respectively. Comparison of Figs 5 and 6 shows that, for the same E_u/s_u ratio, the measured post-jack-in stresses and excess pore pressures show larger deviation from the predicted values than the measured post-installation values. Fig. 7 shows the corresponding measured and predicted peak increment in total stress normal to the active faces of the TSTs and excess pore pressure during the jack-in process. As shown in Fig. 4, this is also approximately the time at which the casing tip reaches transducer elevation during jack-in. As can be seen, the measured peak stress, $\Delta\sigma_{jp}$, and pore pressure, Δu_{jp}, show a much closer agreement with the prediction of plane strain CET than the residual value after complete jack-in.

Figure 8(a) shows the ratios $\Delta\sigma/\Delta\bar{\sigma}$ and $\Delta u/\Delta\bar{u}$ plotted against the depth of the transducer, d_t, normalised by the sand pile diameter, D, for E_u/s_u of 200. As can be seen, the ratios $\Delta\sigma/\Delta\bar{\sigma}$ and $\Delta u/\Delta\bar{u}$ appear to increase with increasing d_t/D ratio. This is not surprising, as in cavity expansion processes plane strain conditions are often approached as the depth increases (e.g. Soderberg, 1962; Banerjee, 1970; Randolph & Wroth, 1979). Based on the amount of surface heave, Randolph & Wroth (1979) suggested that, for a pile driven into soft clay, the plane strain condition is reached when d_t/D exceeds 5. However, there remains substantial scatter between the data points. Figs 8(b) and 8(c) show the same ratios plotted against r_t/D and d_t/r_t, in which r_t is the radial distance of the transducer from the centreline of the SCP. Both figures show an increase in $\Delta\sigma/\Delta\bar{\sigma}$ and $\Delta u/\Delta\bar{u}$ as the radial distance r_t decreases. In particular, Fig. 8(c) shows that $\Delta\sigma/\Delta\bar{\sigma}$ and $\Delta u/\Delta\bar{u}$ increase towards a steady-state value of about 1 as d_t/r_t increases. This suggests that both the radial distance of the transducer and its depth influence the magnitude of the departure from plane strain cavity expansion conditions. As shown in Fig. 9, a similar trend is manifested for E_u/s_u of 120, except that the steady-state value appears to be higher, with many points significantly exceeding 1. For this reason, an E_u/s_u ratio of 200 will be adopted for the back-analyses that follow.

Figure 10 shows the ratios $\Delta\sigma_{jp}/\Delta\bar{\sigma}_j$ and $\Delta u_{jp}/\Delta\bar{u}_j$ corresponding to the measured peak total horizontal stress $\Delta\sigma_{jp}$ and pore pressure Δu_{jp} for the jack-in process, and Fig. 11 shows the corresponding residual values of $\Delta\sigma_j/\Delta\bar{\sigma}_j$ and $\Delta u_j/\Delta\bar{u}_j$. As can be seen, most of the peak values show a similar trend to the post-installation values, increasing to a steady-state value of about 1 at large depth. On the other hand, the band of residual value remains well below 1 even at large depth. This is consistent with the observation of previous researchers, who have found that the stress relief behind the tip of a penetrometer or pile (e.g. Coop & Wroth, 1989) resulted in the set-up stresses being generally lower than that predicted by plane strain CET, even at large depth. This stress relief effect is also consistent with the stress bulb around the tip of a deep penetrometer cone (Levadoux & Baligh, 1980). Fig. 12 shows the measured total radial stress and pore pressure contours inferred from all transducers in all the tests taken together after the casing jack-in. The

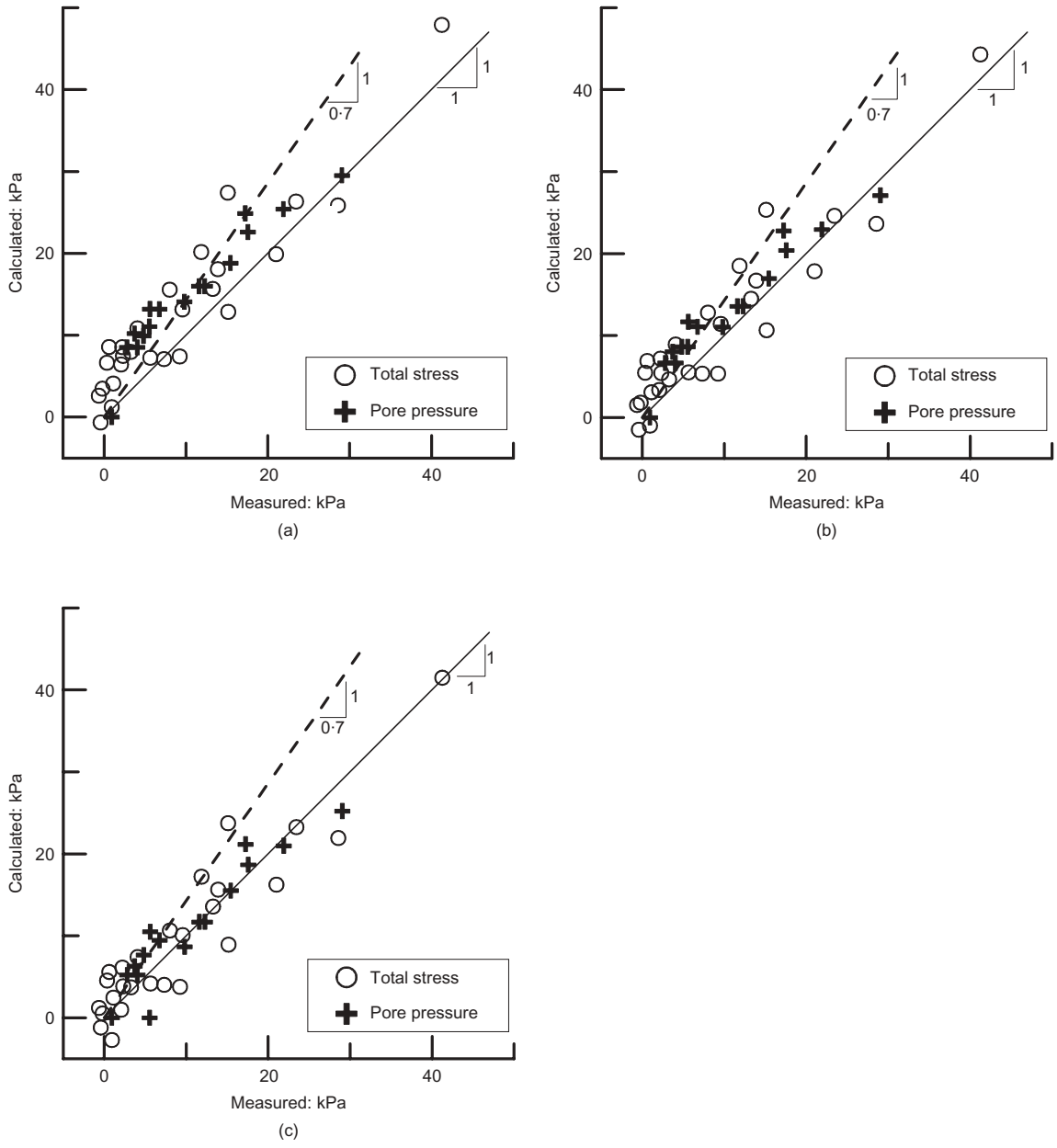

Fig. 5. Calculated against measured increase in total horizontal stress and pore pressure after installation of first SCP in tests T1–T7 using E_u/s_u of: (a) 200; (b) 150; (c) 120

normalised total radial stress and pore pressures are much lower in magnitude than those predicted by Levadoux & Baligh (1980). Note that the Levadoux & Baligh analyses are strictly applicable only to deep penetration situations in which there are no free surfaces or rigid boundaries in the vicinity of the cone tip. These conditions do not really apply to the model tests in which the ground surface is located at a distance of no more than 10 times the casing diameter from the casing tip, and the bottom boundary of the container is located in the vicinity of the casing tip.

Modified cavity expansion theories

One possible reason for the differences between the prediction of plane strain CET and the measured results from the entire installation process is the presence of vertical soil movement, which has been observed in piledriving at small penetration (Randolph & Wroth, 1979), and is manifested as heave at the ground surface. Randolph & Wroth (1979) suggested that allowance could be made for the vertical movement of the soil by reducing the volume of the plastic zone by a factor β. This leads to the radius R_p of the plastic zone (hereafter termed the plastic radius) being reduced by $\sqrt{\beta}$, so that

$$R_p = r_a \sqrt{\left(\frac{\beta G}{s_u}\right)} \tag{1}$$

in which r_a is the radius of the cavity (in this case the SCP) and G is the shear modulus. If σ_r is the radial stress inferred from the measured total stress, and r_t is the distance of the TST from the centreline of the SCP, then the limit pressure, σ_L, can be determined by (e.g. Vesic, 1972)

$$\sigma_L = \sigma_r + 2s_u \ln\left(\frac{r_t}{r_a}\right) \tag{2}$$

The radial stress, σ_R, at the plastic radius R_p is given by

$$\sigma_R = \sigma_0 + s_u \tag{3}$$

in which σ_0 is the in-situ, as well as the far-field radial stress. Combining equations (1), (2) and (3) leads to

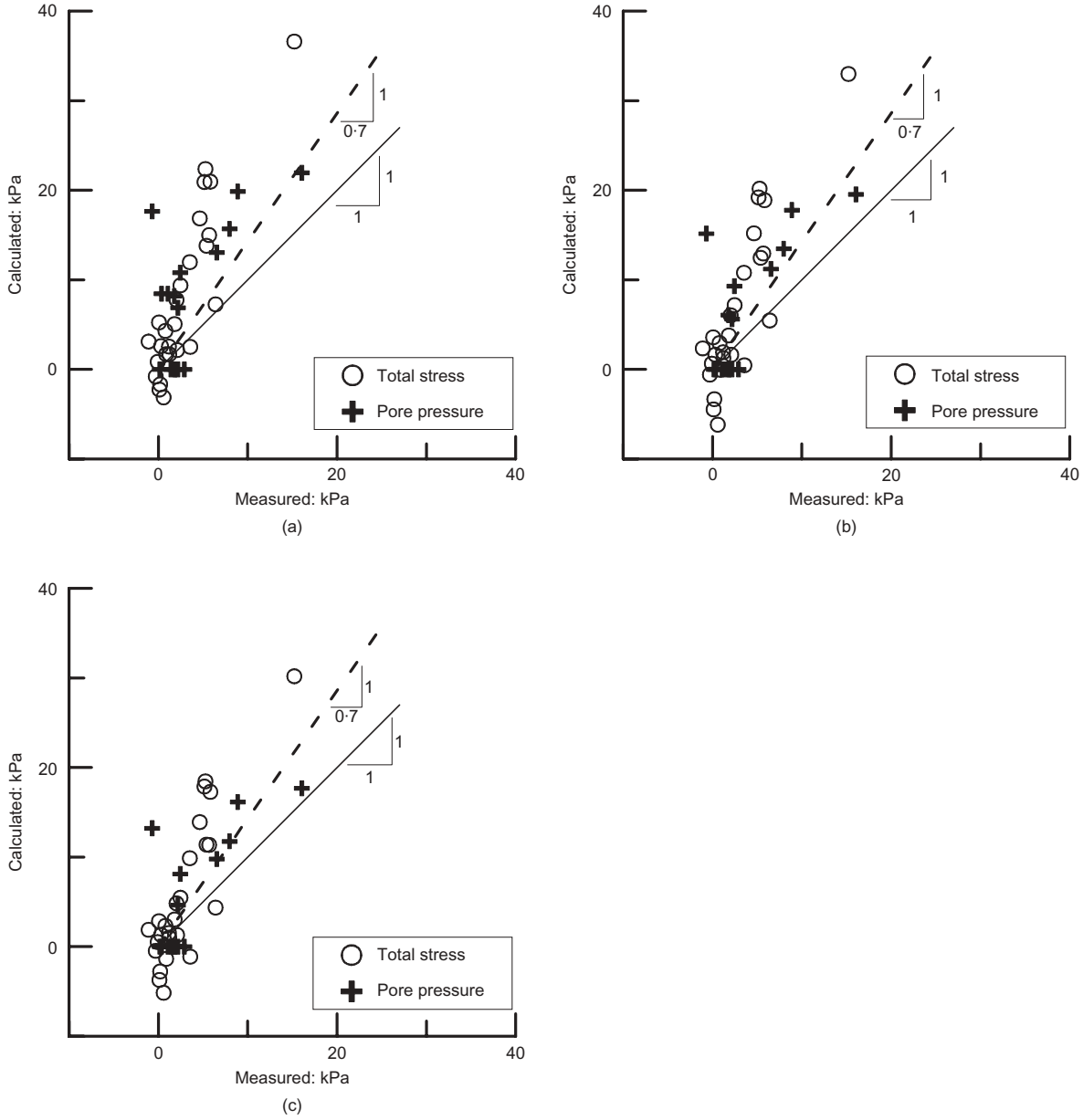

Fig. 6. Calculated against measured increase in total horizontal stress and pore pressure at instant at which casing tip reaches full penetration during installation of first SCP in tests T1–T7 using E_u/s_u of: (a) 200; (b) 150; (c) 120

$$\beta = \frac{s_u}{G}\left(\frac{r_t}{r_a}\right)^2 \exp\left[\frac{\sigma_r - (\sigma_0 + s_u)}{s_u}\right] \quad (4)$$

The procedure used in determining β for each TST is as follows:

(*a*) Starting with the assumption that the TST lies within the plastic zone, infer the radial stress σ_r from the measured horizontal stress through Mohr Circle theory.
(*b*) Compare the radial stress, σ_r, with $\sigma_0 + s_u$. If $\sigma_r > \sigma_0 + s_u$, then the TST is considered to be within the plastic zone. If $\sigma_r < \sigma_0 + s_u$, then the TST lies within the elastic zone. A new value of σ_r is then evaluated assuming an elastic stress field.
(*c*) For TSTs in the plastic zone, equation (4) is used to determine β. For TSTs in the elastic zone, the inferred radial stress at the TST location is used together with elastic CET (e.g. Timoshenko & Goodier, 1970) to determine the radial distance at which the radial total stress is equal to $\sigma_0 + s_u$. This is taken to be the plastic radius, R_p, and equation (1) is then used to determine β.

Depending upon the assumptions made in relation to the shear-induced excess pore pressure, different expressions may be established for the excess pore pressure, Δu. Randolph & Wroth (1979) assumed no shear-induced excess pore pressure whereas Vesic (1972) assumed that there was shear-induced excess pore pressure based on Skempton's pore pressure parameter at failure, A_f. In the back-analysis of the data from the first SCP, Vesic's (1972) theory was adopted, as shear-induced pore pressure is likely to be significant, given that much of the clay is normally or lightly overconsolidated. This leads to

$$\Delta u = \left[0{\cdot}578(3A_f - 1) + 2\ln\left(\sqrt{\frac{\beta G}{s_u}}\frac{r_a}{r}\right)\right] s_u \quad (5)$$

Vesic's (1972) approach predicted a pore pressure discontinuity at the plastic radius. On the inside of the plastic radius, A_f ranges from 0·8 to 1·0 (Dames & Moore, 1983) for Singapore marine clay. In this study, A_f is taken to be 0·8, so that $\Delta u \approx 0{\cdot}81 s_u$ at the plastic radius. On the outside of the plastic zone, $A = \frac{1}{3}$, so that $\Delta u = 0$, as expected. This

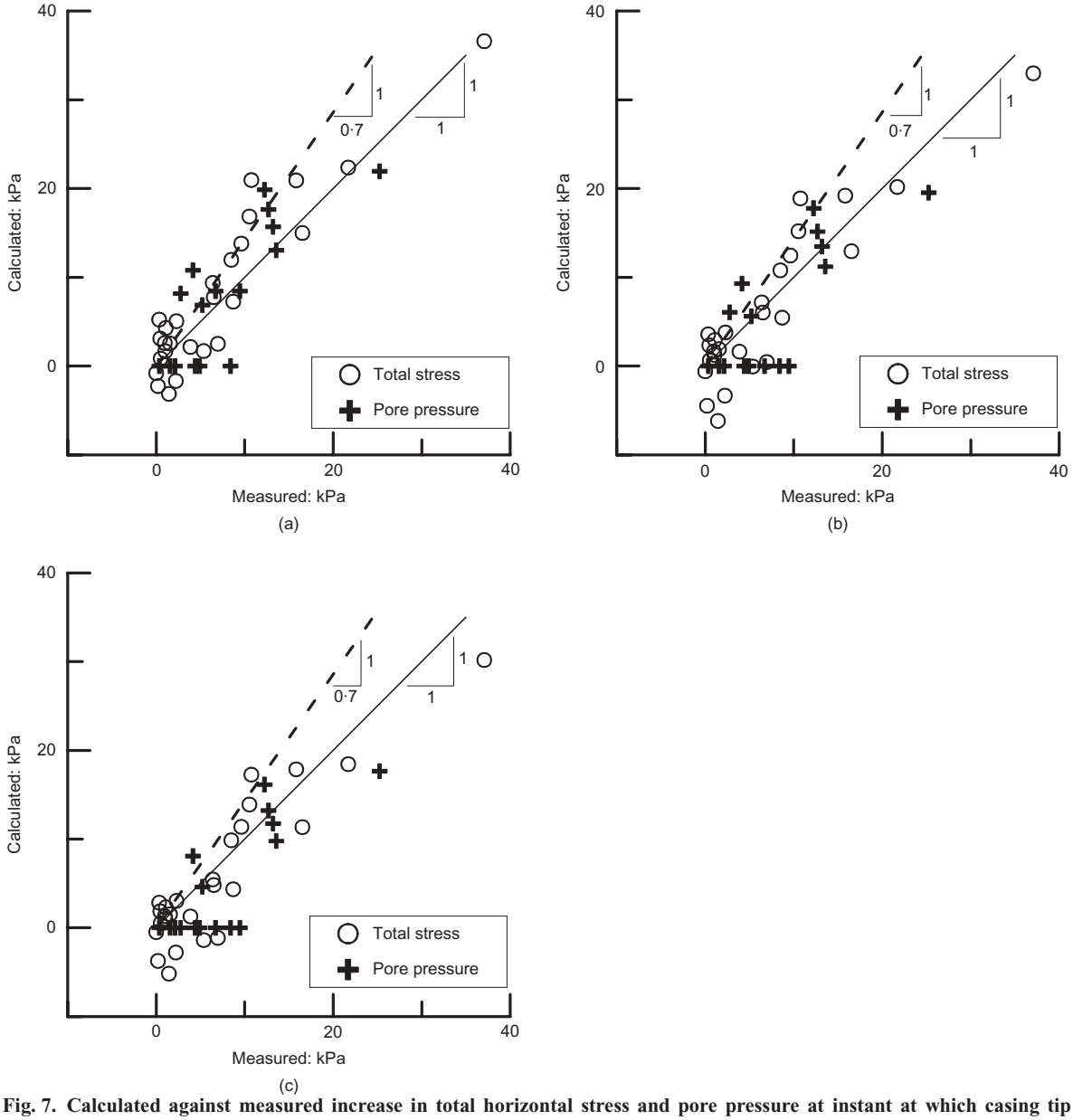

Fig. 7. Calculated against measured increase in total horizontal stress and pore pressure at instant at which casing tip reaches transducer elevation during insertion for installation of first SCP in tests T1–T7 using E_u/s_u of: (a) 200; (b) 150; (c) 120

discontinuity is eliminated if the modified Cam clay model is assumed (Cao *et al.*, 2001). However, as Cao *et al.*'s (2001) results show, the difference is significant only over a small region. In the data analysis, if $\Delta u \geqslant 0{\cdot}81 s_u$, the PPT is considered to be in the plastic zone, and equation (5) is used to deduce β. On the other hand, if $\Delta u < 0{\cdot}81 s_u$, the PPT is considered to be in the elastic zone, and β was not deduced for these points.

Figure 13(a) shows a plot of β values inferred from measured total horizontal stress and excess pore pressures. A trend of increasing β value with depth is quite evident, which is to be expected. However, substantial scatter still remains in the data. This is not surprising, as the radial distance of the transducer, which also has a significant effect on the deviation from the prediction of plane strain CET, is not taken into account in the β-correction.

Effect of free surface on plane strain cavity expansion

Although the variation of β with depth can be determined directly by fitting an intuitively acceptable curve to the data in Figs 5(a) and 6(a), a limiting value of β for shallow depth can be inferred from a semi-theoretical standpoint, and doing so will enhance the theoretical viability of the fit. Heuristically, at very shallow depth, a more probable condition than plane strain is one of constant vertical stress, σ_v. The constancy of σ_v can be considered to be a limiting case of Randolph & Wroth's (1979) 'leakage of soil' concept, as it allows plastic flow to occur in the vertical radial plane without any build-up of vertical stress. As in the case of plane strain CET, the initial stress state is assumed to be isotropic. In plane strain CET, the failure condition within the plastic zone is given by

$$\sigma_r = \sigma_\theta + 2s_u \tag{6}$$

where σ_θ is the tangential stress. Together with the condition of equilibrium, the above leads to the governing equation

$$\sigma_r + 2s_u \ln r + C = 0 \tag{7}$$

in which r is the radial distance from the centre of the cavity, and C is a constant of integration. If, in addition, the vertical stress, σ_v, remains constant, then

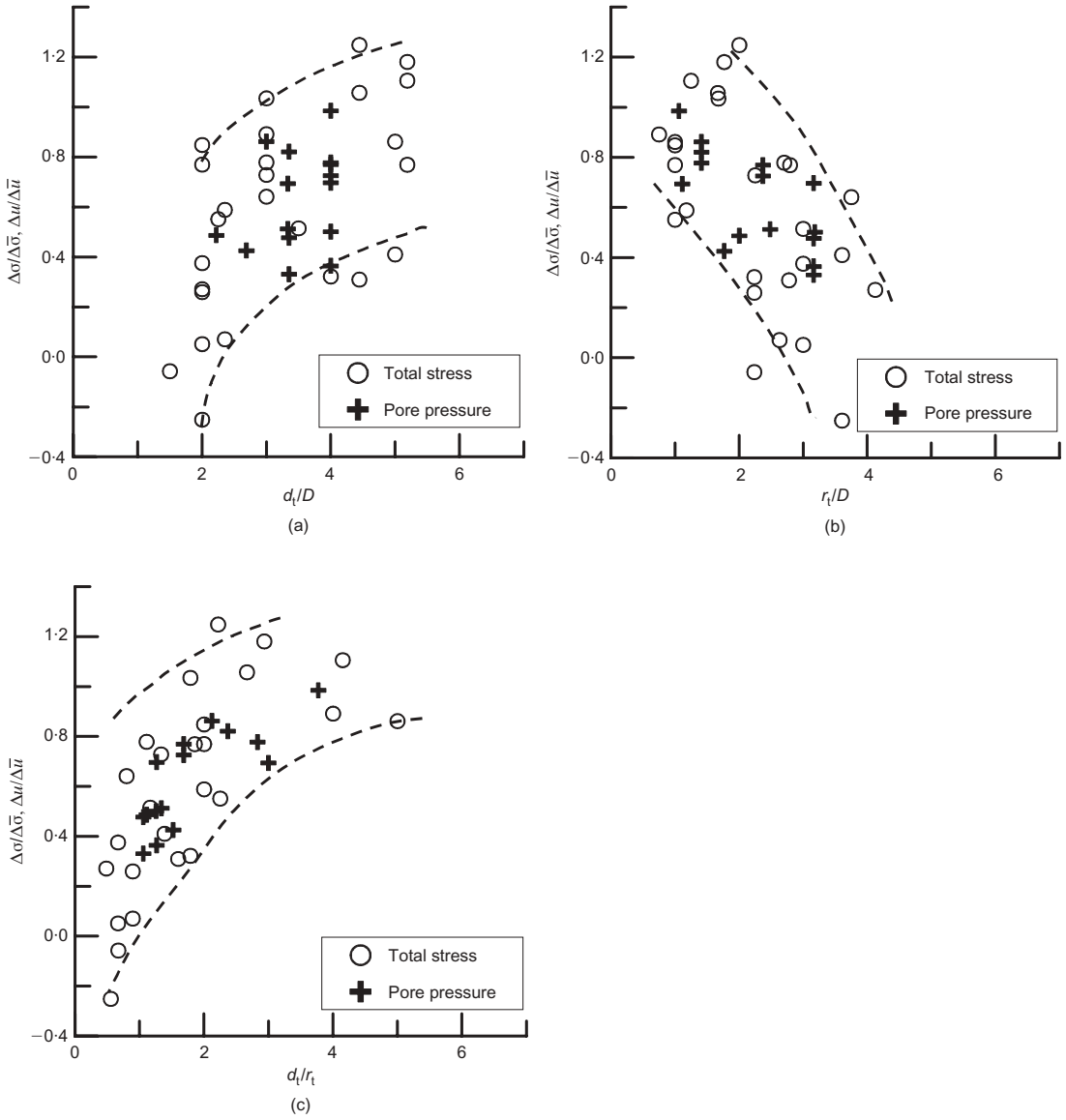

Fig. 8. Variation of measured to calculated increase in total horizontal stress and excess pore pressure ratios after SCP installation for $E_u/s_u = 200$, plotted against: (a) d_t/D; (b) r_t/D; (c) d_t/r_t

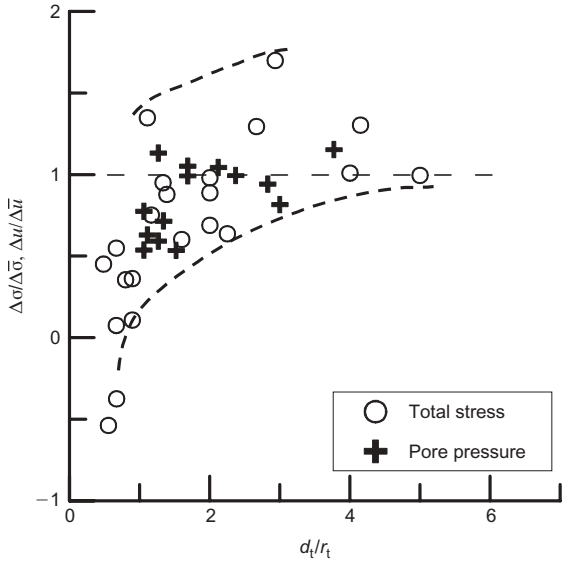

Fig. 9. Variation of measured to calculated increase in stress and excess pore pressure ratios after SCP installation for $E_u/s_u = 120$, plotted against d_t/r_t

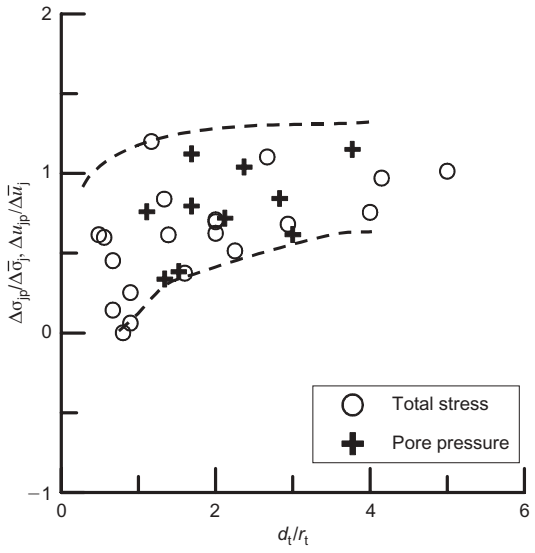

Fig. 10. Variation of measured to calculated increase in stress and excess pore pressure ratios at instant casing had reached transducer elevation for $E_u/s_u = 200$, plotted against d_t/r_t

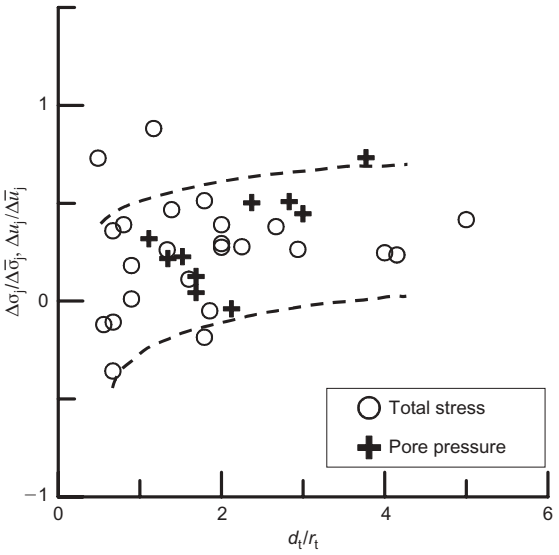

Fig. 11. Variation of measured to calculated increase in stress and excess pore pressure ratios after casing jack-in for E_u/s_u = 200, plotted against d_t/r_t

$$\sigma_r \leqslant \sigma_v + 2s_u \tag{8}$$

which implies that at the cavity wall, i.e. at $r = r_a$,

$$\sigma_r = \sigma_v + 2s_u \tag{9}$$

Combining equation (7) with the boundary condition in equation (9) leads to

$$\sigma_r + 2s_u \ln\left(\frac{r}{r_a}\right) - \sigma_v - 2s_u = 0 \tag{10}$$

At the plastic radius, i.e. $r = R_p$:

$$\sigma_r = \sigma_0 + s_u \tag{11}$$

Substituting the condition in equation (11) into equation (10) leads to

$$R_p = r_a\sqrt{e} \tag{12}$$

The increment in mean total stress, Δp, is given by

$$\Delta p = \frac{2}{3}[\sigma_r - \sigma_0 - s_u] = \frac{2s_u}{3}\left[1 - 2\ln\left(\frac{r}{r_a}\right)\right] \tag{13}$$

Following Vesic (1972), the excess pore pressure is then given by

$$\Delta u = s_u\left\{0{\cdot}578(3A_f - 1) + \frac{2}{3}\left[1 - 2\ln\left(\frac{r}{r_a}\right)\right]\right\} \tag{14}$$

Given that the conditions of constant vertical stress and plane strain represent two opposite extremes of conditions, the variation in limit pressure may be described by a function of the form

$$\sigma_L = \sigma_v + 2s_u + \alpha_1 s_u\left[\ln\left(\frac{G}{s_u}\right) - 1\right] \tag{15}$$

where α_1 is a fitted parameter, which varies between 0 and 1 to allow for the transition from a constant vertical stress condition to a plane strain condition respectively. Substituting equation (15) into equation (2) gives

$$\sigma_r = \sigma_v - 2s_u\left[\ln\left(\frac{r}{r_a}\right) - 1\right] + \alpha_1 s_u\left[\ln\left(\frac{G}{s_u}\right) - 1\right] \tag{16}$$

Similarly, the excess pore pressure may be represented by a similar relationship of the form

$$\Delta u = s_u\left\{0{\cdot}578(3A_f - 1) + \frac{2}{3}\left[1 - 2\ln\left(\frac{r}{r_a}\right)\right] + \alpha_1\left[\ln\left(\frac{G}{s_u}\right) - \frac{2}{3}\left(1 + \ln\left(\frac{r}{r_a}\right)\right)\right]\right\} \tag{17}$$

Substituting the conditions in equation (11) into equation (16) and rearranging the terms yields

$$\frac{R_p}{r_a} = \sqrt{\left(\frac{G}{s_u}\right)^{\alpha_1}\exp(1 - \alpha_1)} \tag{18}$$

from which β can be deduced to be

$$\beta = \left(\frac{G}{s_u}\right)^{\alpha_1 - 1}\exp(1 - \alpha_1) \tag{19}$$

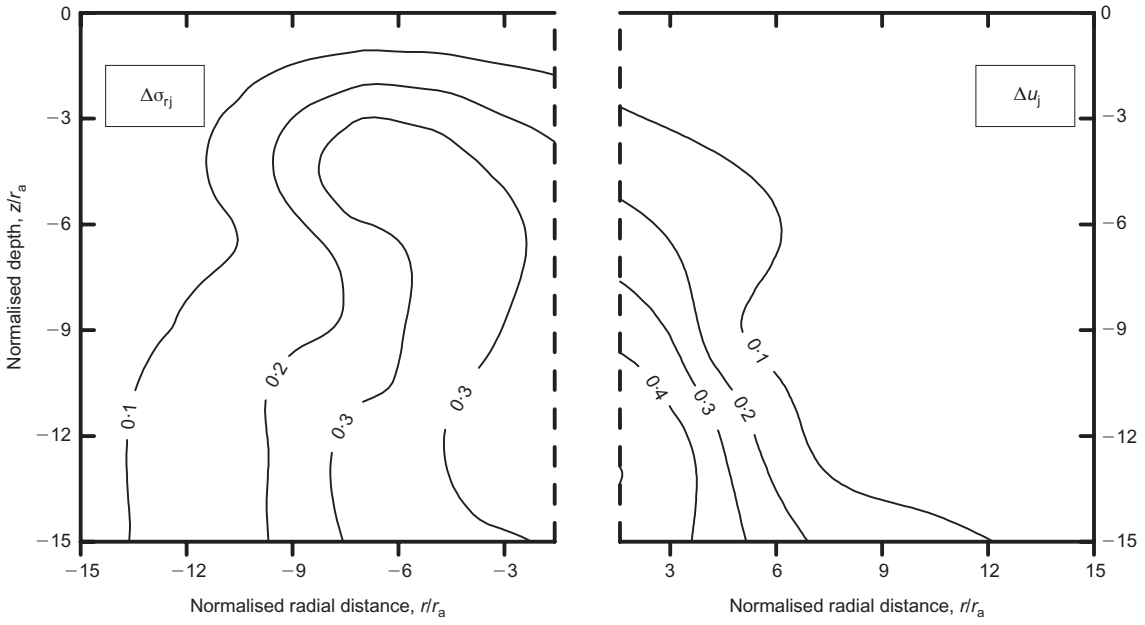

Fig. 12. Measured total radial stress and excess pore pressure contours normalised with effective overburden pressure after jack-in of casing

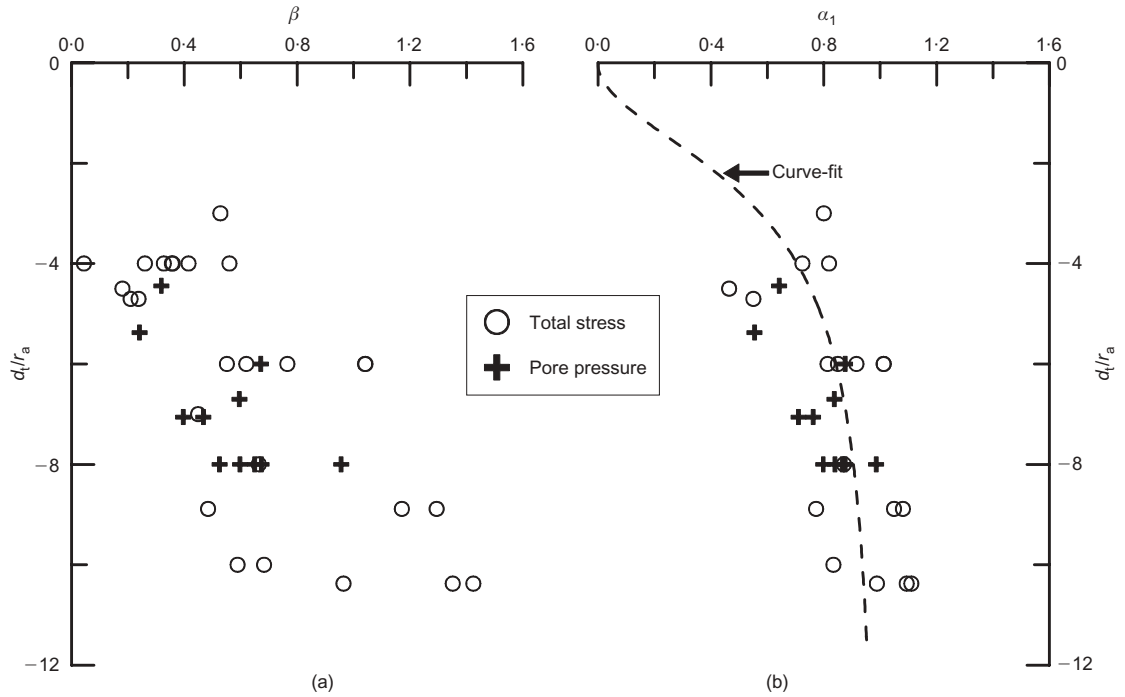

Fig. 13. Variation of reduction factors β and α_1 with depth of transducer: (a) β; (b) α_1

However, in this formulation, β need not be evaluated explicitly, as α_1 can be determined directly by curve fitting.

Figure 13(b) shows the plot of

$$\alpha_1 = \frac{\sigma_L - \sigma_v - 2s_u}{s_u[\ln(G/s_u) - 1]}$$

against d_t/r_a. Following the criteria stated earlier, only transducers with $\sigma_r \geqslant (\sigma_0 + s_u)$ or $\Delta u \geqslant 0{\cdot}81$ (that is, those considered to be in the plastic zone) are used to determine σ_L. In view of equation (15), the fitted curve has to pass through the origin and approach 1 at large depth. As Fig. 13(b) shows, the variation of α_1 with d_t/r_a may be represented by the relation

$$\alpha_1 = \frac{0{\cdot}15(d_t/r_a)^2}{1 + 0{\cdot}15(d_t/r_a)^2} \tag{20}$$

Using the fitted values of α_1, the variation of R_p/r_a with d_t/r_a is plotted in Fig. 14. Also superimposed on this figure are the locations of the transducers, which are represented by different symbols depending on whether they lie within the elastic or plastic zone, based on the total stress and pore pressure criteria proposed earlier. As can be seen, the derived relationship between R_p/r_a and d_t/r_a forms a reasonably good dividing line between the elastic and the plastic locations. This indicates that the semi-empirical way of describing the change in the size of the plastic zone is in reasonably good agreement with the measured data.

The notion of 'soil leakage' discussed above only explains the effect of the depth of the transducer on its measurement; it does not explain the effect of the radial distance. As shown in Fig. 13(b), there remains significant scatter in the α_1 values about the fitted curve, even though the changes in the plastic radius are reasonably well predicted. Fig. 15 shows the contours of $\Delta\sigma_r$ and Δu from the measured data, and Fig. 16 shows the corresponding predicted contours. As can be seen, there is reasonable agreement between the calculated and experimental contours. However, there are also significant differences. First, at radial distances of four times the pile radius, or less, the measured radial stress and excess pore pressure decrease more rapidly than the calculated values as the depth decreases. Second, at the shallower regions, the measured radial stress and excess pore pressure also decrease more rapidly with radial distance than the calculated values. This, and the fact that the plastic radius is reasonably well predicted, indicates that the discrepancy arises from the prediction of stresses and pore pressures within the plastic zone, especially in the shallower region, rather than the size of the plastic zone. Fig. 17 shows the ratios $\Delta\sigma_r/\Delta\bar{\sigma}_{rm}$ and $\Delta u/\Delta\bar{u}_m$ against d_t/r_t, in which $\Delta\bar{\sigma}_{rm}$ and $\Delta\bar{u}_m$ denote the increase in radial stress and excess pore pressure calculated using equations (16) and (17). Although Fig. 17 shows a more rapid approach of the ratios

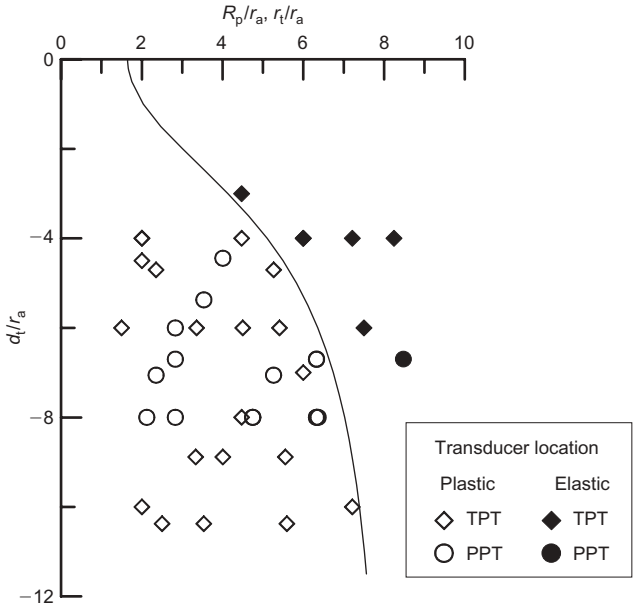

Fig. 14. Variation of plastic radius along depth with transducer locations superimposed

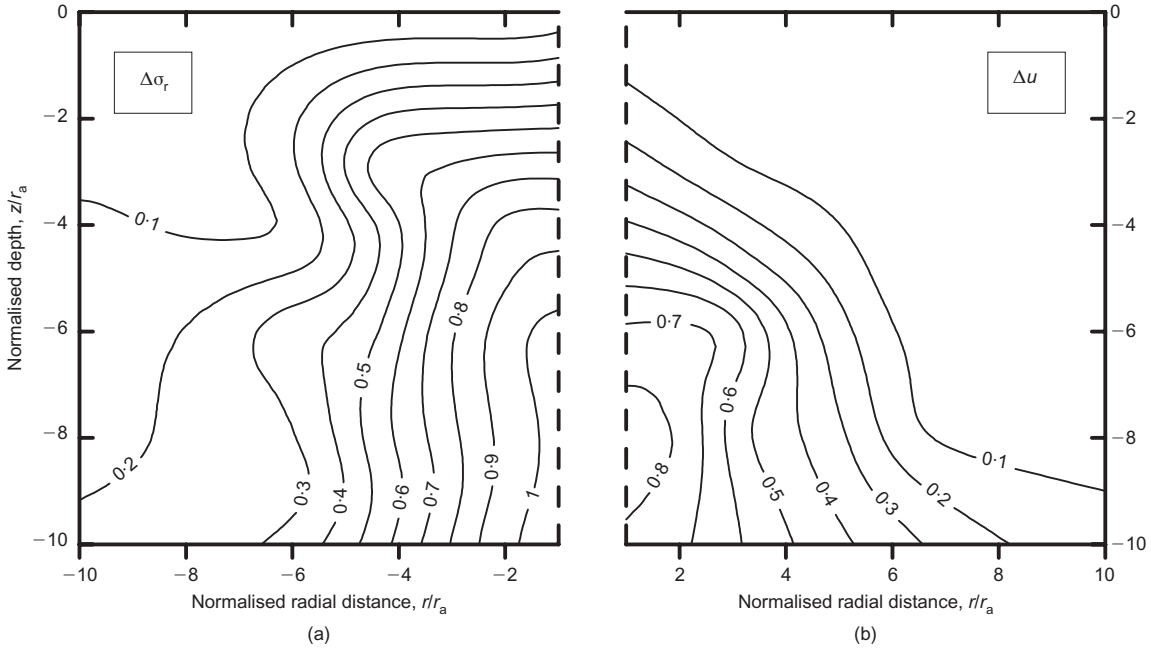

Fig. 15. Measured total radial stress and pore pressure contours normalised with effective overburden pressure after installation of SCP

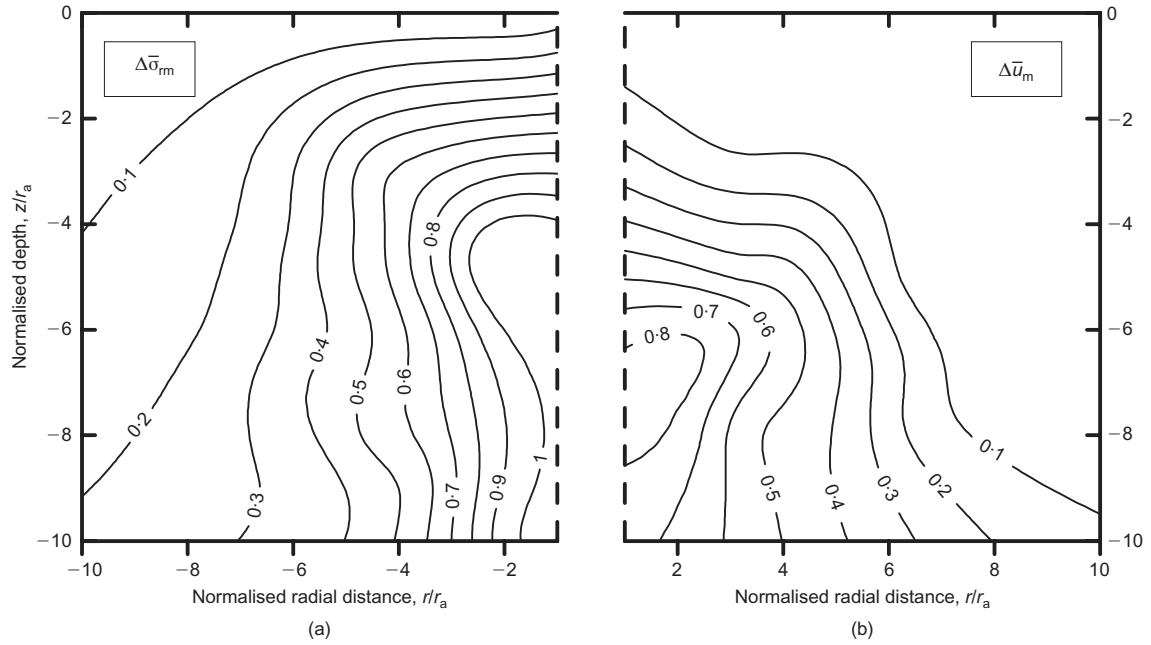

Fig. 16. Predicted total radial stress and pore pressure contours normalised with effective overburden pressure after installation of SCP

$\Delta\sigma_r/\Delta\overline{\sigma}_{rm}$ and $\Delta u/\Delta\overline{u}_m$ towards the steady-state value, nevertheless the dependence on d_t/r_t still exists. The strongly trended variation of the ratios $\Delta\sigma_r/\Delta\overline{\sigma}_{rm}$ and $\Delta u/\Delta\overline{u}_m$ with d_t/r_t suggests that the discrepancy seen in Fig. 13(b) is deterministic rather than stochastic in nature, and is also unlikely to be due to experimental errors. One possible cause of this discrepancy is the presence of shear stress τ_{rv}, which is induced in the vertical radial plane by the differential upward motion of the soil in the plastic zone. The effect of these shear stresses cannot be readily incorporated within the framework of plane-strain CETs; however, the results do permit semi-empirical relations to be fitted to the data in Fig. 17 to take account of the effect of d_t/r_t, which modify equations (16) and (17) to:

$$\sigma_r = \sigma_v + \frac{(d_t/r_t)^{3\cdot33}}{1+(d_t/r_t)^{3\cdot33}} \times \left\{\alpha_1 s_u\left[\ln\left(\frac{G}{s_u}\right)-1\right]-2s_u\left[\ln\left(\frac{r}{r_a}\right)-1\right]\right\} \quad (21)$$

and

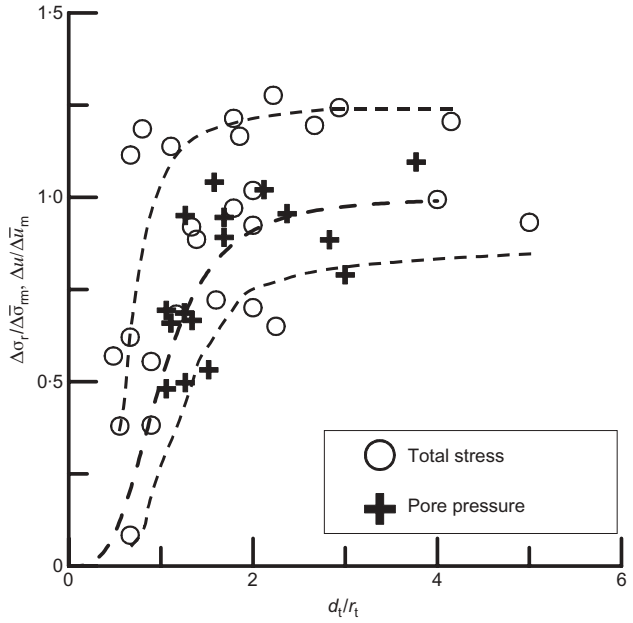

Fig. 17. Ratio of measured to 'modified' calculated increase in total radial stress and pore pressure after SCP installation, plotted against d_t/r_t

$$\Delta u = \frac{(d_t/r_t)^{3\cdot33}}{1+(d_t/r_t)^{3\cdot33}}\left\{0\cdot578(3A_f-1)+\frac{2}{3}\left[1-2\ln\left(\frac{r}{r_a}\right)\right]\right.$$
$$\left.+\alpha_1\left[\ln\left(\frac{G}{s_u}\right)-\frac{2}{3}\left(1+\ln\left(\frac{r}{r_a}\right)\right)\right]\right\}s_u \qquad (22)$$

Figure 18(a)–(c) compares the measured peak jack-in, post-jack-in and post-installation stress increase and excess pore pressure with the corresponding calculated values using equations (21) and (22). Comparison of Fig. 18(c) with Fig. 5(a) shows much tighter banding of the post-installation values about the line of equality, indicating that the data can be accommodated within a highly deterministic framework, if the salient factors are accounted for. Comparison of Fig. 18(a) with Fig. 7(a) shows that there is also a tightening in the banding of the peak jack-in values, even though the fitting has not been conducted on the peak jack-in values. This suggests that the factors affecting the entire installation process and the jack-in process may be quite similar. However, the post-jack-in values remain significantly overestimated.

Effect of installing multiple piles in a grid

As shown in Fig. 3, in the model tests the SCPs are installed in groups, with the number of piles in each group ranging from two to nine. The centre-to-centre spacing between piles in the groups ranges from 1·5 to 2·5 times the SCP diameter. This corresponds to an area replacement ratio (Aboshi & Suematsu, 1985) of between 12·6 and 35%. This replacement ratio is lower than that often used in practice (e.g. Aboshi & Suematsu, 1985; Wei, 1997), and is dictated largely by the need to have sufficient soft clay around the transducers. Moreover, there has also been increasing interest in SCPs with lower replacement ratios (e.g. Rahman *et al.*, 2000). Fig. 19 compares the total horizontal stress and pore pressure increase measured during the installation of each of the subsequent piles with the total radial stress and pore pressure inferred from equations (21) and (22). As can be seen, the radial stress increase due to the installation of each

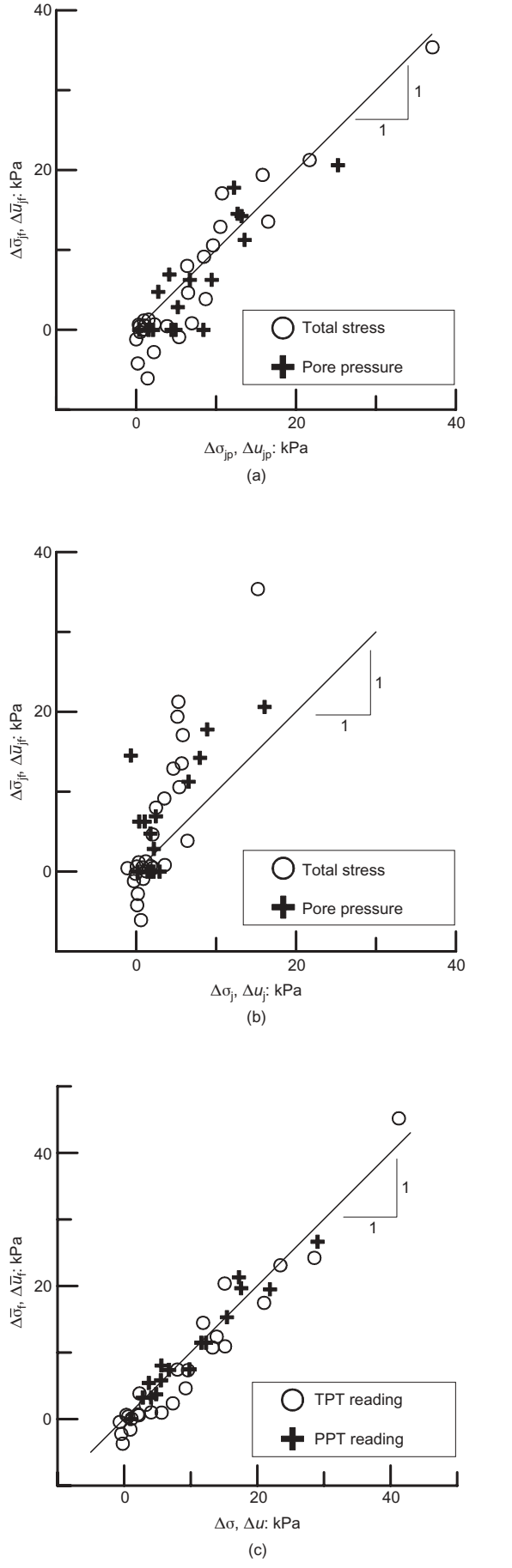

Fig. 18. Variation of measured stress and pore pressure against calculated values inferred from 'modified' CET: (a) peak jack-in; (b) post-jack-in; (c) post-installation

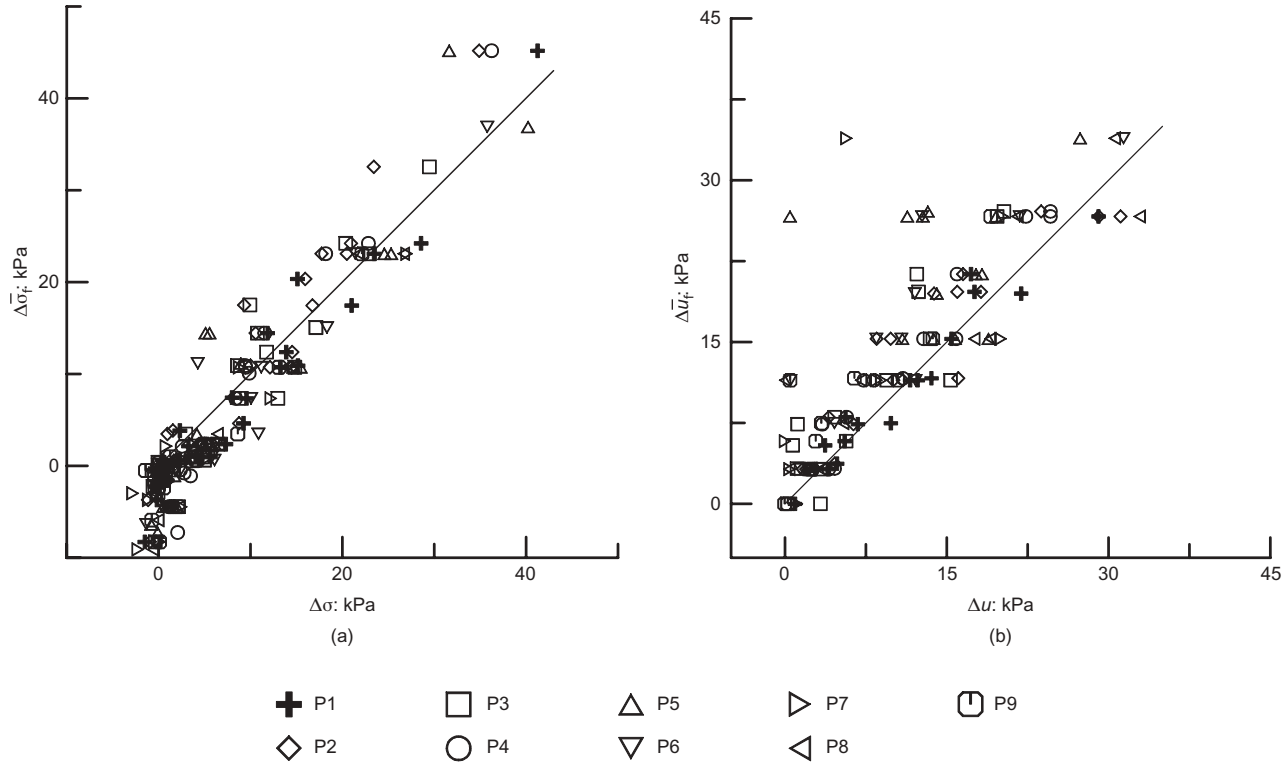

Fig. 19. Variation of measured stress increase and excess pore pressure due to installation of SCP group, plotted against calculated values inferred from 'modified' CET: (a) total stress normal to TST; (b) excess pore pressure

of the subsequent pile remains reasonably well predicted by equation (21), even though the state of the ground has already been altered by the piles that have been installed. As discussed earlier, horizontal stress acting on the transducer is inferred by first computing the radial stress increment using equation (21). The tangential stresses are then computed using equation (6) if the transducer is in the plastic zone, and

$$\sigma_\theta = \sigma_v - s_u\left(\frac{R_p}{r}\right)^2 \tag{23}$$

if the transducer is in the elastic zone. Hence the fact that the radial stress increment is reasonably well predicted implies that the cumulative increase in radial stress may be reasonably estimated by accumulating the radial and tangential stress changes from the current pile onto the pre-existing state stress at the point in question, and then applying Mohr's circle transformation to evaluate the stress in the required direction. On the other hand, Fig. 19(b) shows that the increment in pore pressure is largely overestimated for second and subsequent sand piles in the grid. This may be attributed to the possibility that much of the shear-induced excess pore pressure might have been developed during the installation of the first pile. Therefore installation of the second and subsequent pile may only generate excess pore pressure due to the total stress changes rather than shear induction. Fig. 20 compares the measured pore pressure increment with that calculated using equation (22) without the shear-induced component; this assumption is the same as that of Randolph & Wroth (1979) for pile driving. As can be seen, the pore pressure increment is now largely underestimated. This suggests that some shear-induced component may still be present for the second and subsequent piles. This may be attributed partly to the fact that some of the soil at locations, which are far away from the first SCP of the grid, might not have reached critical state during the installation of the first SCP. In addition, some amount of reconsolidation of the soft clay would have taken place during SCP installation. Such reconsolidation processes will probably bring the state of the soil away from the critical state by increasing the effective stress and reducing the deviator stress.

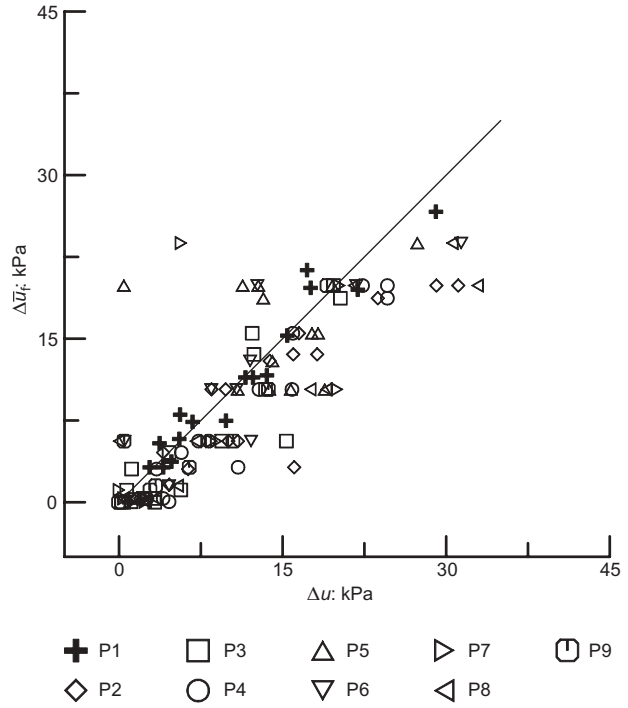

Fig. 20. Comparison of measured excess pore pressure with that calculated without shear effect in second and every subsequent SCP installation

CONCLUSIONS

The discussion above has presented laboratory data relating to the radial stress and pore pressure set-up of the ground in the process of sand compaction pile installation, which will pave the way towards a more rational description of the state, and thereby the performance, of the improved ground after installation of sand compaction piles. Back-analysis of the post-installation data shows that plane-strain cavity expansion theory appears to give a reasonably good estimate of the build-up in pore pressure and total radial stress at large depths, but significantly overestimates the build-up in pore pressure and total radial stress at shallow depth. The deviation from the estimates by plane strain cavity expansion theory is dependent upon the depth and radial distance. Somewhat better matching was obtained using a semi-empirical correction, which is based on two limits: plane strain at large depth and constant vertical stress nearer to the ground surface. However, there remains a significant radial distance effect, which cannot be explained by plane cavity expansion theories alone.

The peak jack-in radial total stress increment and excess pore pressure follow a similar trend to the post-installation values, when compared with cavity expansion theory. However, the residual jack-in radial total stress and pore pressure are much smaller than those predicted by cavity expansion theory. This can be explained by the stress relief that follows in the wake of a blunt penetrator being pushed into the ground.

These findings imply that, in order to mobilise significant set-up of stress in the improved ground, there must be substantial further cavity expansion during the sand injection stage of sand pile installation. Installing a sand pile that has the same diameter as the casing is unlikely to mobilise much set-up in the ground. It also means that, for the same sand pile diameter, a smaller casing is likely to be able to generate larger set-up than a larger casing.

The data presented also indicate that the cumulative radial total stress increment at a given location due to the installation of multiple piles in a grid may be reasonably estimated by superimposing the increments due to the installation of each pile. On the other hand, pore pressure build-up is shown to be less readily superimposed, possibly because the shear-induced component of excess pore pressure does not increase linearly and infinitely with deviator stress.

ACKNOWLEDGEMENTS

The authors are grateful to Dr H. Aboshi, Dr M. Nozu and Dr M. Randolph for providing some very relevant literature during the course of this research. They also wish to thank the National University of Singapore (NUS) for financial support and the use of equipment under research grant R-264-000-059-112.

NOTATION

- A_f Skempton's pore pressure parameter
- D SCP diameter
- d_t depth of transducer
- E_u Young's modulus
- g gravitational acceleration field
- R TST registration ratio
- R_p radius of plastic zone around SCP
- r radial distance of point from centre of cavity
- r_a radius of SCP
- r_c radius of casing
- r_t radial distance of transducer from centre of SCP
- s_u undrained shear strength of clay
- t elapsed model time from the instant the casing starts to jack-in
- u pore pressure measured (including ambient pressure)
- z depth below model surface
- β, α_1 reduction factors
- σ total stress measured normal to active TST diaphragm
- σ_0 in-situ horizontal/radial stress
- σ_r total radial stress
- σ_θ total tangential stress
- σ_v total vertical stress
- σ_L limit pressure at cavity wall/ultimate cavity pressure
- σ_R radial stress at plastic radius
- $\Delta\sigma$ total stress increment measured normal to active TST diaphragm
- $\Delta\bar{\sigma}$ total stress increment calculated normal to active TST diaphragm
- $\Delta\sigma_r$ total stress increment measured in radial direction
- $\Delta\bar{\sigma}_r$ total stress increment calculated in radial direction
- Δu excess pore pressure (measured)
- $\Delta\bar{u}$ excess pore pressure (calculated)

Subscripts

- f calculated after SCP installation using equations (21) and (22)
- j after casing jack-in
- jf calculated after casing jack-in using equations (21) and (22)
- jp peak measured value during jack-in
- m calculated using α_1

REFERENCES

Aboshi, H. & Suematsu, N. (1985). Sand compaction pile method: state-of-the-art paper. *Proc. 3rd Int. Sem. Soil Improvement Methods, Singapore*, 1–12.

Aboshi, H., Ichimoto, E., Enoki, M. & Harada, K. (1979). The composer: a method to improve characteristics of soft clays by inclusions of large diameter sand columns. *Proceedings of the international conference on soil reinforcement: reinforced earth and other techniques*, Paris, Vol. 1, pp. 211–216.

Aboshi, H., Mizuno, Y. & Kuwabara, M. (1991). Present state of sand compaction pile in Japan. In *Deep foundation improvement: design construction and testing* (eds M. I. Esrig and R. C. Bachus), ASTM STP 1089, pp. 32–46. Philadelphia: American Society for Testing and Materials.

Almeida, M. S. S., Davies, M. C. R. & Parry, R. H. G. (1985). Centrifuge tests on embankments on strengthened and unstrengthened clay foundations. *Géotechnique* **35**, No. 4, 425–441.

Asaoka, A., Kodaka, T. & Nozu, M. (1994). Undrained shear strength of clay improved with sand compaction piles. *Soils Found.* **34**, No. 4, 23–32.

Banerjee, P. K. (1970). *A contribution to the study of axially loaded pile foundations*. PhD thesis, University of Southampton, UK.

Cao, L. F., Teh, C. I. & Chang, M. F. (2001). Undrained cavity expansion in modified Cam clay I: Theoretical analysis. *Géotechnique* **51**, No. 4, 323–334.

Coop, M. R. & Wroth, C. P. (1989). Field studies of an instrumented model pile in clay. *Géotechnique* **39**, No. 4, 679–696.

Dames & Moore (1983). *Singapore mass rapid transit system: Detailed geotechnical study interpretative report*. Singapore: MRTS.

Enokido, M., Takahashi, Y., Gotoh, S. & Maeda, K. (1973). The restoration of disturbed clay ground due to sand compaction pile driving. *Tsuchi-to-Kiso* (Jpn Soc. Soil Mech. Found. Engng) **29**, No. 5, 13–20 (in Japanese).

Gibson, R. E. & Anderson, W. F. (1961). In-situ measurements of soil properties with the pressuremeter. *Civ. Engng Public Works Rev.* **56**, No. 658, 615–618.

Kimura, T., Nakase, A., Kusakabe, O. & Saitoh, K. (1985). Behaviour of soil improved by sand compaction piles. *Proc. 11th Int. Conf. Soil Mech. Found. Engng*, San Francisco, USA, **2**, 1109–1112.

Konig, D., Jessberger, H. L., Bolton, M., Phillips, R., Bagge, G., Renzi, R. & Garnier, J. (1994). Pore pressure measurement during centrifuge model tests: Experience of five laboratories. *Proceedings of the International Conference Centrifuge 94* (eds

C. F. Leung, F. H. Lee and T. S. Tan), pp. 101–108. Rotterdam: Balkema.

Kitazume, M., Miyajima, S. & Nishida, Y. (1996). Stability of revetment on soft clay improved by SCP. *Proc. 2nd Int. Conf. Soft Soil Engineering*, Nanjing, China **2**, 455–460.

Lee, F. H., Ng., Y. W. & Yong, K. Y. (1996). Centrifuge modelling of sand compaction piles in soft ground. *Proc. 2nd Int. Conf. Soft Soil Engineering*, Nanjing, China **2**, 407–412.

Lee, F. H., Ng., Y. W. & Yong, K. Y. (2001). Effects of installation method on sand compaction piles in clay in the centrifuge. *Geotech. Test. J.* **24**, No. 3, 314–323.

Lee, F. H., Juneja, A., Tan, T. S., Yong, K. Y. & Ng, Y. W. (2002a). Excess pore pressure due to sand compaction pile installation in soft clay. *Proceedings of the international conference on physical modelling in geotechnics*, St John's, Canada pp. 955–960.

Lee, F. H., Juneja, A., Wen, C., Dasari, G. R. & Tan, T. S. (2002b). Performance of total stress cells in model experiments in soft clays. *Proceedings of the international conference on physical modelling in geotechnics*, St John's, Canada 101–106.

Leung, C. F., Lee, F. H. & Yet, N. S. (2001). Centrifuge model study on pile subject to lapses during installation in Sand. *Int. J. Phys. Modelling Geotech.* **1**, No. 1, 47–57.

Levadoux, J. N. & Baligh, M. M. (1980). *Pore pressures during cone penetration in clays*, Research Report R80-15. Cambridge, MA: Department of Civil Engineering, Massachusetts Institute of Technology.

Ng, Y. W., Lee, F. H. & Yong, K. Y. (1998). Development of an in-flight sand compaction piles (SCPs) installer. *Proceedings of the international conference Centrifuge 98* (eds T. Kimura, O. Kusakabe and J. Takemura), Vol. 1, pp. 837–843. Rotterdam: Balkema.

Rahman, Z., Takemura, J., Kouda, M. & Yasumoto, K. (2000). Experimental study on deformation of soft clay improved by low replacement ratio SCP under backfilled caisson loading. *Soils Found.* **40**, No. 5, 19–35.

Randolph, M. F. & Wroth, C. P. (1979). An analytical solution for the consolidation around a driven pile. *Int. J. Numer. Anal. Methods Geomech.* **3**, 217–229.

Robinson, R. G., Tan, T. S. & Lee, F. H. (2003). A comparative study of suction induced seepage consolidation versus centrifuge consolidation. *Geotech. Test. J.* **26**, No. 1, 92–101.

Sekiguchi, H. & Ohta, H. (1977). Induced anisotropy and time dependency in clays. *Proc. 9th Int. Conf. Soil Mech. Found. Engng, Tokyo*, Specialty Session 9, 229–237.

Soderberg, L. O. (1962). Consolidation theory applied to foundation pile time effects. *Géotechnique* **12**, No. 3, 217–225.

Takada, N., Ohshima, A., Mikasa, M. & Kawamoto, K. (1988). Centrifuge model tests on anchored sheet pile quay wall on clay ground. *Proceedings of the international conference Centrifuge 88* (ed. J.-F. Corte), pp. 233–242. Rotterdam: Balkema.

Timoshenko, S. P. & Goodier, J. N. (1970). *Theory of elasticity*, 3rd edn. New York: McGraw-Hill.

Vesic, A. S. (1972). Expansion of cavities in infinite soil mass. *J. Soil Mech. Found. Div. ASCE* **98**, No. SM3, 265–290.

Wei, J. (1997). Ground improvement techniques: the HDB way. *Proceedings of the international conference on ground improvement techniques*, Macau, pp. 609–619.

Weiler, W. A. Jr & Kulhawy, F. H. (1982). Factors affecting stress cell measurements in soil. *J. Geotech. Engng Div., ASCE* **108**, No. GT12, 1529–1548.

Yong, K. Y., Karunaratne, G. P. & Lee, S. L. (1987). Recent developments in soft clay engineering in Singapore. *Proceedings of the conference on urban coastal area management*, Singapore, pp. 3–10.

Yu, H. S. (2000). *Cavity expansion methods in geomechanics*. Dordrecht: Kluwer Academic.